EPAPS

Drag moderation by the melting of ice surface in contact with water

Ivan U. Vakarelski[1*], Derek Y. C. Chan[2,3], and Sigurdur T. Thoroddsen[1]

[1] Division of Physical Sciences and Engineering & Clean Combustion Research Center, King Abdullah University of Science and Technology (KAUST), Thuwal 23955-6900 Saudi Arabia.

[2] School of Mathematics and Statistics, University of Melbourne, Parkville VIC 3010 Australia.

[3] Department of Chemistry and Biotechnology, Swinburne University of Technology, Hawthorn, VIC 3122 Australia.

[*]ivanuriev.vakarelski@kaust.edu.sa

1. Production of the ice-shell-metal-core spheres.

The method of making the ice-shell-metal-core "ice(metal)" spheres using an ice-mold is illustrated schematically in Fig. S1a. In brief, a metallic sphere is suspended inside the centre of the spherical void of an aluminium mold. The space between the metallic sphere and the mold wall is filled with water before the mold is placed inside a temperature controlled chamber (Fig. S1b). After the water has frozen, the mold is taken out of the chamber and left for some time to condition at room temperature. Finally the top part of the mold is removed as shown in Fig S1c and the ice(metal) sphere is released from the mold.

The aluminium molds were custom produced in KAUST machine workshop. The mold has a spherical void diameter of 60 mm and can accommodate a spherical metallic core of up to 40 mm in diameter. The mold has two parts: top-half and base-half that fit together to form a perfect spherical void (Fig. S1a). The inside surface of the mold is polished to a fine finish of average surface roughness < 0.1 mm. After suspending the metal sphere inside the mold, the top and base parts are tighten together by four connecting bolts (Fig. S1). At the top of the mold there is a 6.0 mm opening that is used to fill it with water and through which the metal sphere can be suspended.

For the metallic core we used a range of tungsten carbide (ρ_s = 14.9 g/cm^3, D_s = 20, 30, 40 and 45 mm) or stainless steel (ρ_s = 7.7 g/cm^3, D_s = 20, 30 and 40 mm) spheres purchased from FRITSCH GmbH, (Germany) or from Zhuzhou Goode Tungsten Carbide Co., Ltd (China). Using an electric discharge machine a 1.0 mm hole was drilled at the top of the spheres and a hook ending metallic wire was fitted inside. The metallic wire is used to suspend the sphere inside the mold and to handle the ice(metal) spheres without the need to touch the ice surface (Fig. S1).

To freeze the water we use an ESPEC, SH-261 bench-top temperature & humidity chamber (ESPEC Corp., Osaka, Japan). The chamber temperature range is from –60 ^{0}C to +100 ºC. In a standard run we kept the mold for at least 2 hours inside the chamber at a temperature of –10 ºC, that allows the water to freeze completely. Alternatively, temperatures range from –5 ºC to –20 ºC was also used to freeze the water with lower temperature requiring longer freezing time (e.g. overnight for –5 ºC).

Following freezing the mold is taken out of the chamber and left to condition for some time at room temperature. During the conditioning period, the mold is put on top of an inverted Nalgene plastic tray to minimise the heat exchange between the base and the bench (Fig. S1c). We time the release of the ice(metal) sphere from the mold from the moment when the outer surface of the ice(metal) sphere starts to melt. This is done to ensure that a thin water layer covers the sphere when it was released from the mold, preventing the formation of frost on the ice surface and thus keeping the surface smooth. To characterize the room temperature conditioning process we mounted 3 thermocouple probes at control points inside the mold, inside the ice shell and inside the metal sphere core as indicated in Fig. S2a. Variation of the temperatures with time is measured using a thermocouple thermometer temperature logger (OM-SQ2010-KIT, Omega Engineering). Such time variations for spheres frozen at –10 ºC and –20 ºC are shown in Fig. S2b. The ice(metal) sphere is released from the mold at about the time the mold temperature reaches zero. At this time the shell and core temperatures are only slightly below zero (between –2 ºC and 0 ºC) as evident from Fig. S2b. Releasing the ice(metal) spheres from the mold in this manner ensure that the temperatures of the mold wall, the ice shell and the metal core will be the same for all freeze temperatures.

Fig. S3 together with Fig. 1 in the manuscript show the appearance of the ice(metal) spheres after being released form the mold. If we use fresh de-ionised (DI) water the ice appears milky (Figs. S3a, S3b), and that is due to the presence of dissolved air in the water resulting in the formation of tiny bubble inclusions in the ice. If the DI water was de-aerated by first boiling for about 30 minutes before use for ice making, the ice appears transparent with only a small number of discrete bubble inclusions. Such bubbles are not

located near the external surface of the ices shell (Fig. S3c, see also Fig. S7 and manuscript Fig. 1). In test measurements, we found the fall velocity to be independent of the appearance of the ice. However, to ensure that the smoothness of the ice surface is not affected by the release of micro-bubbles during the slow melting of the ice, boiled de-aerated water was used to produce ice(metal) spheres.

2. **Spheres free fall in water experiments**

The water tank in which the sphere fall experiments were conducted was 2 meter tall and has a cross section of 30 cm × 30 cm (180 liters). The tank is made of clear Acrylic with a wall thickness of 10 mm. A second tank of slightly larger dimension: 2.4 meter tall and with cross section of 40 cm × 40 cm (384 liters) was used for the heaviest sphere or higher Reynolds number experiments.

Following the release from the ice mold, the ice(metal) sphere was quickly moved to the water tank and carefully released from rest at just below the water surface at the top of the tank. The sphere fall in the tank was recorded with a high speed camera (Photron Fastcam SA-5) with a typical framing rate of 1000 fps. Variation of the ice(metal) sphere position with time and the corresponding velocity were determined by image processing the videos with the camera software (Photron FASTCAM Viewer, PFV Ver.3262).

The ice(metal) spheres fall velocities were compared with solid metal spheres fall velocities. In a set of experiments we used stainless steel spheres of various diameters (ρ_s = 7.7 g/cm^3, D_s = 20, 25, 30, 40, 50 and 60 mm). Complementary experiments were conducted using a 60 mm diameter hollow alumina sphere inside which smaller diameter spheres can be fitted to exactly match the weights of the 60 mm ice(metal) spheres used (see Fig. S4). Comparing the fall velocity of ice(metal) and solid metal spheres of identical radius and mean density gives an accurate estimate of the melting ice surface effect. Supplemental video 1 demonstrates an example of the parallel fall of ice(metal) and solid metal spheres of identical size and weight.

The drag coefficient C_D, was determined form the terminal velocity U_T of the sphere of diameter D using the relation:

$$C_D = (4[\rho_s - \rho]gD)/(3\rho U_T^2) \quad [1]$$

where, g is the gravitational acceleration, ρ the water density and ρ_s the sphere density. The terminal velocity was corrected for the effect of the tank walls using the following correction formula due to Newton (1687):

$$U_T/U_{T\infty} = [1-(D/D_c)^2]\,[1-0.5(D/D_c)^2]^{1/2} \quad [2]$$

where U_T is the measured terminal velocity, $U_{T\infty}$ is the corrected terminal velocity for an infinite flow domain, D is the sphere diameter and D_c is the diameter of a cylindrical tank. For the $a \times a$ square cross-section tank used in the present experiment, the effective diameter D in eq. 2 is calculated by equating the areas of the circle and the square, i. e. $D_c = \left(2/\sqrt{\pi}\right)a$.

For spheres released from rest, the time dependence of the velocity, $U(t)$ is observed to evolve towards the terminal value, U_T according to the exponential form [S1]:

$$U(t) = U_T(1 - e^{-t/\tau}) \quad [3]$$

This equation does not accurately present the complex dynamic of the true fall trajectory, but could be used as an effective tool to estimate the terminal velocity. Results for the drag coefficient shown in the manuscript Fig. 3 are calculated using the sphere velocity measured close to the bottom of the tank. Each data point is the average of at least three independent experimental runs with error bars representing the typical data spread in these measurements. For higher Reynolds number ice spheres ($Re > 2 \times 10^5$) the velocity at the tank bottom has not yet reached the terminal value as demonstrated by the data in Fig. 2 of the manuscript. In all cases, the drag coefficients of the ice(metal) sphere

calculated from the velocity at the tank bottom shown in Fig. 3 of the manuscript represent upper bound estimates.

To conduct experiments at a lower temperature, we first filled about 1/3rd of the tank with ice cubes produced by an ice-making machine (Scotsman CU2026SA, Prodigy©). The tank was then filled to top with room temperature DI water. After mixing and melting of the ice cubes it was possible to achieve water temperature in the tank of about 6 ± 1 ºC. The kinematic viscosity of water at 6 ºC is about 1.47 $\times 10^{6}$ m^{2} s^{-1} compared to 0.97 $\times 10^{6}$ m^{2} s^{-1} at 22 ºC. This effectively limits the experimental range of accessible Reynolds number with our experimental setup from $Re \sim 3 \times 10^{5}$ in 22 ºC water to $Re \sim 1.7 \times 10^{5}$ in 6 ºC.

3. **Cooled sphere free fall experiments**

To evaluate the effect of water cooling by being in contact with the ice(metal) sphere we conducted a series of experiments using 60 mm solid steel spheres preconditioned by cooling in the temperature chamber in the temperature range of –30 ºC to +20 ºC. Spheres that were cooled to temperature below zero rapidly became covered by a frost layer once exposed to the laboratory atmosphere. Before their release in water these solid steel spheres were defrosted by a brief wash with ethanol (freezing temperature –114 ºC) that removes frost layer and the ethanol wetted sphere surface prevents further frost formation as demonstrated in Fig. S5. There were no visible sign of ice layer forming on the sphere surface during the rapid fall in water. Results from these experiments are presented in Fig S6. They show that the terminal velocity of solid steel spheres is independent of the sphere temperature in the range –30 ºC to +20 ºC. Shown for comparison is the apparent terminal fall velocity of ice(metal) spheres of the same size and weight prepared using freezing temperatures in the range –20 ºC to –5 ºC. However, due to the ice sphere conditioning process explained in the previous sections the actual temperature of all of ice(metal) spheres in the fall experiment is close to 0 ºC.

The chamber temperature used to cool the sphere is only one possible measure of the temperature of the sphere during the fall in water. To make a more detailed characterization we used a sphere with thermocouple probe fitted inside hole drilled at the sphere top (at about 10 mm below the surface). A long fine wire connects the thermocouple probe to the temperature logger to facilitate measurement the sphere temperature during the fall in water. The temperature chronology of such experiment is shown in Fig. S7 that tracks the temperature progression from when the sphere is taken out of the temperature chamber, washed in ethanol, release to fall in water to the bottom of the tank and then rapidly pulled out of the tank. For this data we could estimate that for spheres cooled at chamber temperature –20 ºC, the sphere temperature during the fall is between –15 ºC to –10 ºC. In all cases the sphere temperature is below zero during the fall and we anticipate a stronger cooling of the surrounding water compared to case the ice(metal) sphere whose temperature is always close to zero in our experiments.

4. **Estimation of the sphere melting rates**

The melting rate of ice spheres during the fall in room temperature water was estimated by comparing high magnification back illumination images (shadow images) of the ice(metal) sphere when it is at the beginning of the fall and when it is near the bottom of the tank. Technically this was accomplished using two synchronized high-speed cameras, one focused on the top part and the other on the bottom part of the tank. Fig. S8 shows the results of such experiments, with the images of the sphere at the tank top (Fig. S8c) and near the bottom (Fig. S8d). These images are used to estimate the change in the sphere diameter. In a series of such experiments we established a characteristic melting rate of the diameter of falling spheres has magnitude: $|dD/dt| = 0.6 \pm 0.2$ mm/s. For comparison we also undertake measurements with spheres held stationary in the water, and established a typical melting rate which is about one order of magnitude lower, e.g. about $|dD/dt| = 0.08$ mm/s (see Fig. S8a and Fig. S8b).

The melting rate on sphere falling in 6 ºC water was too low to allow precise measurement in the time-scale of the experiments. However, for static spheres in 6 ºC water we measured $|dD/dt| = 0.0045$ mm/s, or melting rate was about 18 times lower than the rate for room temperature water.

We noticed that during the course of the ice(metal) sphere fall experiment, the amount of surface melting is very small with no detectable deviation from the spherical shape and the ice surface remains smooth. Thus the observed drag reduction is not due to deviations from the spherical geometry as a result of differential surface melting or the development of surface geometric features as the ice surface melts. However, if the ice spheres were permitted to travel a significant distance, one would expect shape change due to melting as another mechanism for altering drag.

5. Visualization of the ice sphere wake

To visualize the ice sphere wake we added a water-based red dye (AFFCO, Red Food dye) at about 3 vol % to the water used to prepare the ice. In all cases the fall velocity of the dyed ice(metal) sphere was found to be identical with the fall velocity of the pure water ice(metal) sphere. From this we concluded that the dye at the concentration used has no effect on the drag on the ice(metal) spheres. The visualization of the wake of a 60 mm ice(metal) sphere falling at velocity corresponding to lower $Re \sim 5 \times 10^4$ and higher $Re \sim 1.5 \times 10^5$ is shown in Supplemental Video 2.

6. Mechanism of the early onset of drag reduction

Before considering the physical mechanism underlying the observed of drag reduction of ice spheres of radius R travelling at constant velocity U in a quiescent Newtonian fluid of shear viscosity, μ, we recapitulate the general characteristics of the drag coefficient, C_D of a sphere in the range of Reynolds number, $Re = 2\rho RU/\mu \sim 10^4 - 10^6$. In this regime, the drag is due to the pressure or inertial contribution, also known as the form or wake drag, with skin friction accounting for less than 5% of the total drag. For $Re < 2 \times 10^5$, C_D is relatively constant in the range 0.4 – 0.5 but drops rapidly at $Re \approx 2.5 \times 10^5$, to about 0.1 – 0.2 corresponding to a drag reduction [S1 – S3]. This is called the 'drag crisis' and is associated with the change in the nature of the boundary layer that affects the position of its separation from the surface of the sphere. For $Re < 2 \times 10^5$, the boundary layer on the forward portion of the sphere is laminar and separates near the equator (90º from the front of the sphere) and leads a wide wake behind the sphere where the low pressure cannot compensate the pressure at the forward portion. As Re increases beyond 2×10^5, the laminar boundary layer begins to transition into a turbulent boundary layer on the forward surface. The turbulent boundary layer carries more momentum so that laminar boundary layer can remain attached to the sphere surface beyond the equator, separating downstream at around 120º from the front of the sphere. The resulting wake is therefore much narrower, so that more of the pressure on the forward portion of the sphere is thus partially compensated, thus giving rise to a lower drag [S2].

Fundamentally, all drag reduction mechanisms of a sphere moving in a Newtonian fluid involve moving the point of flow separation to the rear portion of the sphere surface to generate a narrower wake. However the underling physical mechanisms that can trigger the early onset of the drag crises transition differ. A number of drag reduction strategies have been reported in the literature:

- Addition of small amounts of flexible polymers to induce non-Newtonian visco-elastic behavior in the fluid that alters the behavior of the boundary layer [S3, S4],

- Adding physical features to the surface such as golf ball dimples, trip wires, shark skin riblets to trigger the onset of turbulence in the boundary layer at lower *Re* [S5].

- Creating a low density and low viscosity layer near the surface by sustaining a Leidenfrost vapor layer or a plastron gas layer on the surface [S6, S7], that changes the non-slip boundary condition to a partial or full slip boundary condition in order to reduce friction between the viscous boundary layer and the surface.

In this paper, we showed that a *microscopic* scale chemical phenomenon of phase change or melting of an ice surface, resulting in the local mass transfer of 'new' fluid at the solid-fluid interface, can also cause drag reduction on a *macroscopic* scale associated with moving the point of flow separation to the rear portion of the sphere.

To relate this process to a more familiar paradigm of what happens at the fluid-solid boundary, we can view this either as:

(i) a partial-slip effect due to the melting of the surface, e. g. the rate of the surface melting, $|dR/dt|$ acts as a slip velocity U_S to which an effective slip length, λ_S can be associated, or

(ii) an effective local thickening of the viscous boundary layer due to mass transfer of water from the melting surface, e.g. $|dR/dt|$ is considered as the velocity at which the boundary layer is effectively increasing in thickness as fluid flows past the surface.

6.1 Estimation of the slip length vs. boundary layer thickness

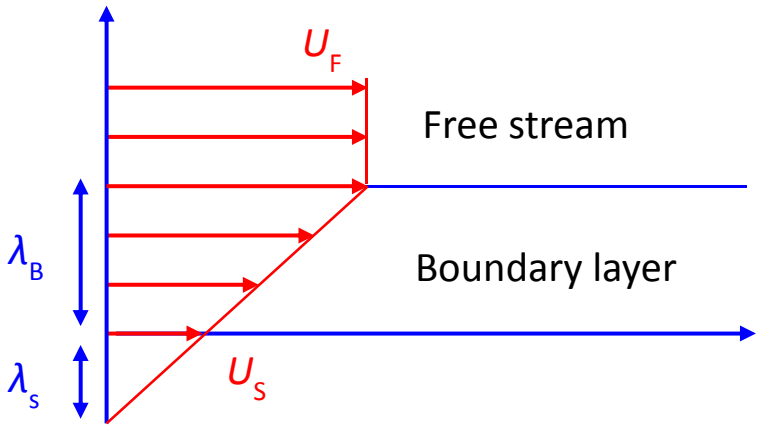

Schematics 1. Schematics of the boundary layer velocity field variation: U_F in the free stream velocity; U_S is the fluid velocity at the surface; λ_B is the viscous boundary layer thickness, and λ_S is the slip length defined as the extrapolation depth at which the velocity vanishes.

Schematics 1 shows the velocity field variation from the free stream value, U_F to U_S slip velocity at the solid surface, illustrating the standard definition of the slip length, λ_S as the extrapolated position of apparent zero velocity [S7]. For simplicity we have drawn a linear velocity profile but the same scaling argument will hold for non-linear profiles:

$$\lambda_S/(\lambda_B + \lambda_S) \sim U_s/U_F \qquad [4]$$

In the case of the of boundary layer developing on a melting surface we can assume that the slip velocity to scale with the melting rate of the surface, or $U_s \sim |dR/dt|$ for the case of our melting ice sphere. The free stream velocity around the sphere will have a radial dependence, but will scale with the sphere terminal velocity, or $U_F \sim U_T$. Then for the

case of the melting sphere: $U_s/U_F \sim |dR/dt|/U_T$. Taking the typical values measured values of $|dR/dt| \sim 0.3$ mm/s and $U_T \sim 2$ m/s ($Re \sim 1.2 \times 10^5$) we estimate that:

$$\lambda_S / \lambda_B \sim 0.0015 \qquad [5]$$

The typical slip length is about three orders of magnitude smaller than the boundary layer thickness. This estimate indicates that unlike the case of the Leidenfrost or plastron vapor layers [S6, S7] the typical slip length due to the melting surface is much smaller than then the boundary layer thickness and the partial slip could not explain the range of the drag reduction observed.

6.2 Estimation of the melting thickness vs. boundary layer thickness

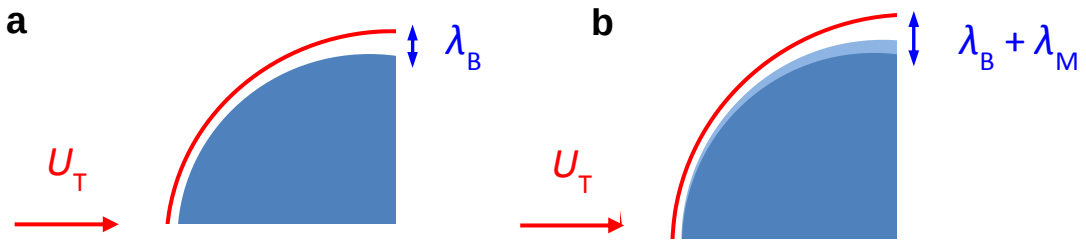

Schematics 2. Schematics of the boundary layer around: (a) a solid sphere and (b) melting sphere in which case the thickness of the boundary layer, λ_B is effectively increased by λ_M due to the mass transfer of water from the surface. The lighter gray color in (b) is to illustrate the freshly melted water from the ice surface mixing with the boundary layer. Notice that for the time scale of our experiments $\lambda_M << R$, so the spherical shape of the sphere is not compromised.

Schematic 2 is illustrates the effect of the mass transfer from the melting surface as an effective thickening of the viscous boundary layer. To quantify this effect we introduce a

characteristic melting thickness, λ_M defined as the thickness change of the ice layer as the sphere move over a distance of one diameter, D. From the above melting experiments, we estimate the melting rate of falling ice(metal) spheres to be $|dR/dt| \sim 0.3$ mm/s. Thus a characteristic melting thickness scale is:

$$\lambda_M \sim |dR/dt| \, (D/U_T) \sim 10 \ \mu m \qquad [6]$$

for a sphere of diameter $D \sim 60$ mm with a terminal velocity $U_T \sim 2$ m/s. This is smaller than, but of similar order to the characteristic thickness of the boundary layer, λ_B estimated as [S8]:

$$\lambda_B \sim D / Re^{1/2} \sim 170 \ \mu m \qquad [7]$$

for the same sphere at a Reynolds number, $Re \sim 1.2 \times 10^5$.

Although λ_M is estimated to be only 5-10% of thickness of the boundary layer on a solid sphere, this appears to be sufficient to increase the momentum in the viscous boundary layer to allow the point of separation from the surface to be moved towards the rear of the sphere that leads to the early onset of the drag crisis observed in our experiment.

A further confirmation of the hypotheses that the melting surface rate is the key physical parameter come from experiment conducted in low temperature 6 ºC water, in which case the melting rate is about 20 times lower and the drag reduction effect is fully suppressed.

The above analysis necessarily simplistic given limited experimental evidence adduced from the present study. However, we hope that our initial investigations will stimulate further experimental, theoretical and computational studies to better quantify and understand this intriguing phenomenon.

References

S1. N. Lyotard, W.L. Shew, L. Bocquet, and J.-F. Pinton, Eur. Phys. J. B **60**, 469 (2007).

S2. E. Achenbach, J. Fluid Mech. **54**, 565 (1972).

S3. A. White, Nature **216**, 994 (1967).

S4. C. M. White and M. G. Mungal, Annu. Rev. Fluid Mech. **40**, 235 (2008).

S5. H. Choi, W-P. Jeon, and J. Kim, Annu. Rev. Fluid Mech. **40**, 113 (2008).

S6. I. U. Vakarelski, J. O. Marston, D. Y. C. Chan, and S. T. Thoroddsen, Phys. Rev. Lett. **106**, 214501 (2011).

S6. C. Cottin-Bizonne, J.-L. Barrat, L. Bocquet, and E. Charlaix, Nature Mater. **2**, 237 (2003).

S8. S. Tomotika, Aero. Res. Comm. Rept. and Memo. No. 1678, 86 (1937)

Supplemental Videos Legends

Supplemental Video 1. A comparison of a 60 mm diameter ice(metal) sphere (left) and of a 60 mm diameter solid metal sphere (right) of the same weight corresponding to a mean density ρ_s = 7.8 g/cm^3, falling in room temperature (22 ºC) water. The videos are taken at the lower part of the tank where the spheres approach terminal velocity. The frame rate used was 1000 fps and the video playback speed is 30 fps. See also Fig. 2 in the manuscript.

Supplemental Video 2. A comparison of the rate of fall of 60 mm diameter ice(metal) spheres with different size metallic cores in 22 ºC water. A red dye has been added to the ice forming water to visualize the wake behind the falling spheres. On the left side the sphere velocity ~ 0.8 m/s corresponding to Re = 5×10^4 and on the right side is ~ 2.4 m/s corresponding to Re = 1.5×10^5. The frame rate used was 1000 fps and the video playback speed is 30 fps

Supplemental Video 3. A comparison of a 60 mm diameter ice(metal) sphere (left) and of a 60 mm diameter solid composite metal sphere (right) of the same weight corresponding to a mean density ρ_s = 8.9 g/cm^3, falling in 6 ºC water. The videos are taken at the lower part of the tank where the spheres approach terminal velocity. The frame rate used was 1000 fps and the video playback speed is 30 fps.

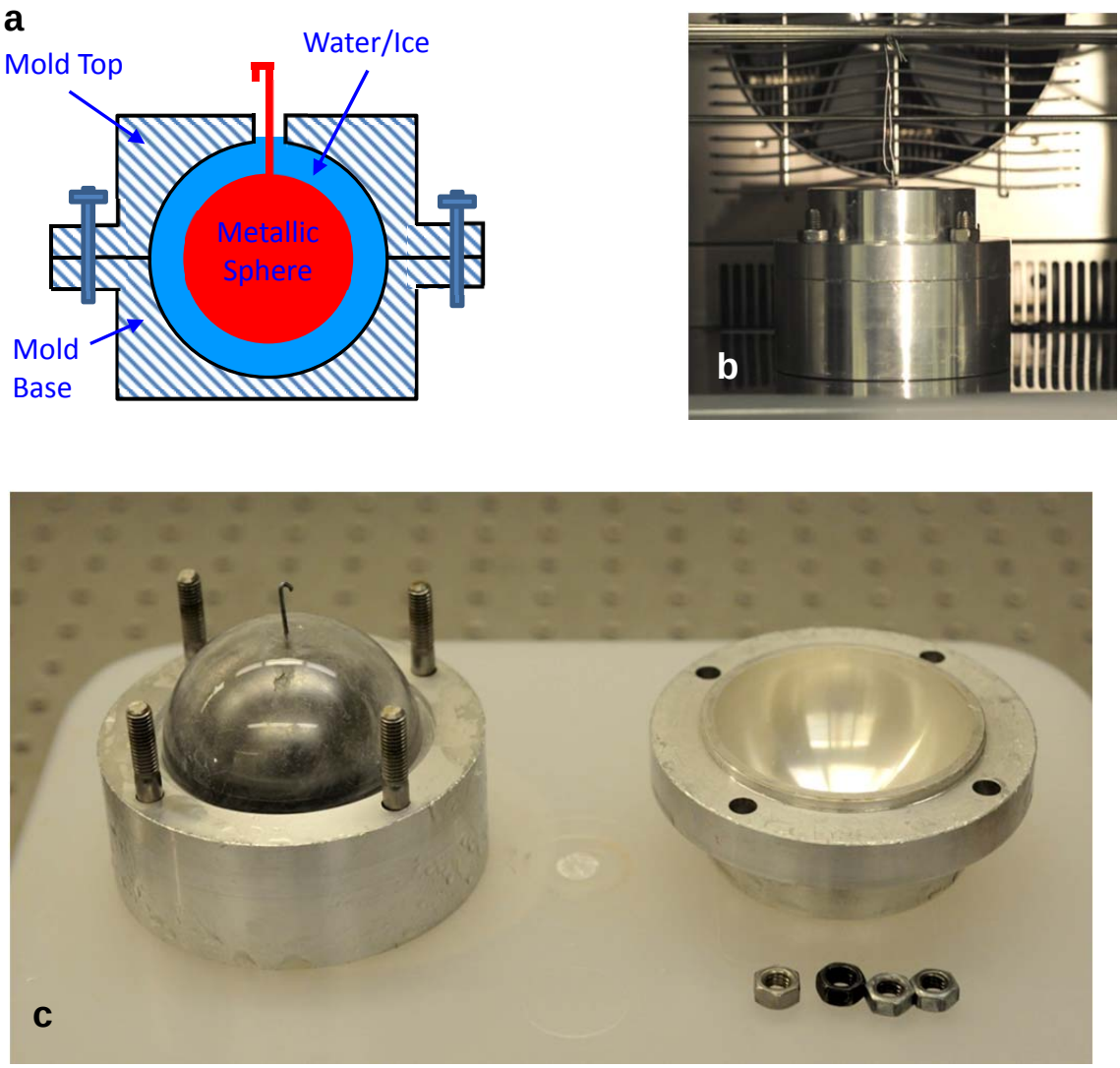

Supplemental Figure S1. (a) A schematic of the ice-shell-metal-core "ice(metal)" spheres prepared in an aluminium mold. (b) Photograph of the aluminium mold set inside the environmental chamber. (c) Photograph of the ice mold with the ice sphere inside shortly after removal of the mold top.

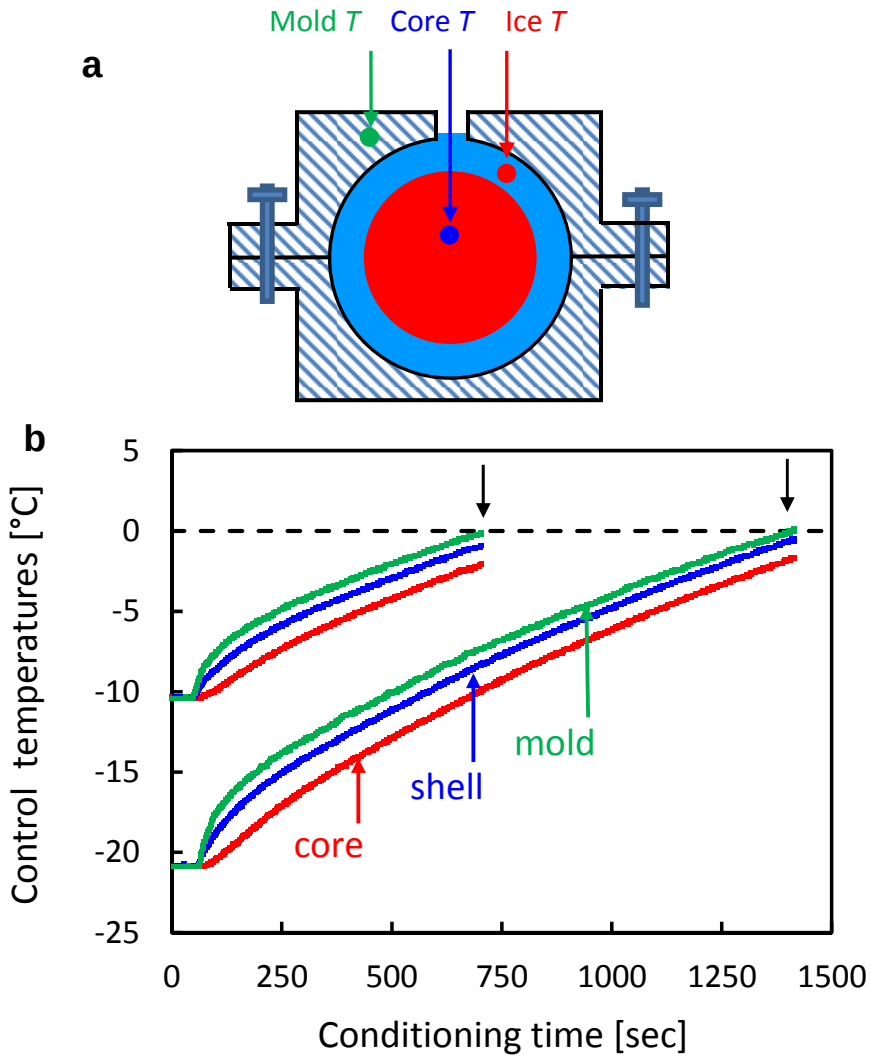

Supplemental Figure S2. (a) Schematic showing the placement of the 3 thermocouple probes: inside the mold wall (green), inside the ice shell (blue) and inside the metal core (red) (b) Time variations of the temperature at the three control point (same colors as in part (a)) for a freezing temperature of –10 ºC and –20 ºC. Arrow indicates the approximate time when the ice(metal) spheres are removed from the mold.

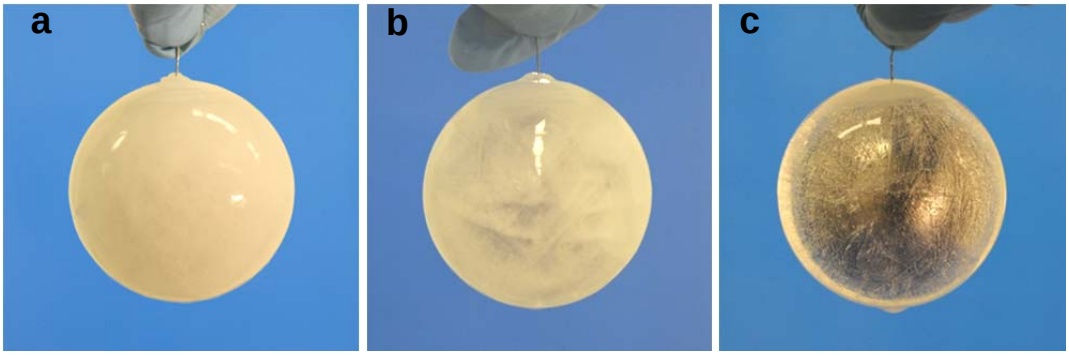

Supplemental Figure S3. Photography of a 60 mm diameter ice(metal) sphere. In all cases, the metallic core is a 40 mm diameter steel sphere. (a) Using DI water, freezing temperature –20 ºC (b) using DI water freezing temperature –10 ºC (c) using DI water de-aerated by boiling, freezing temperature –5 ºC. The sphere fall velocity is identical for all spheres and does not depend on the appearance of the ice shell.

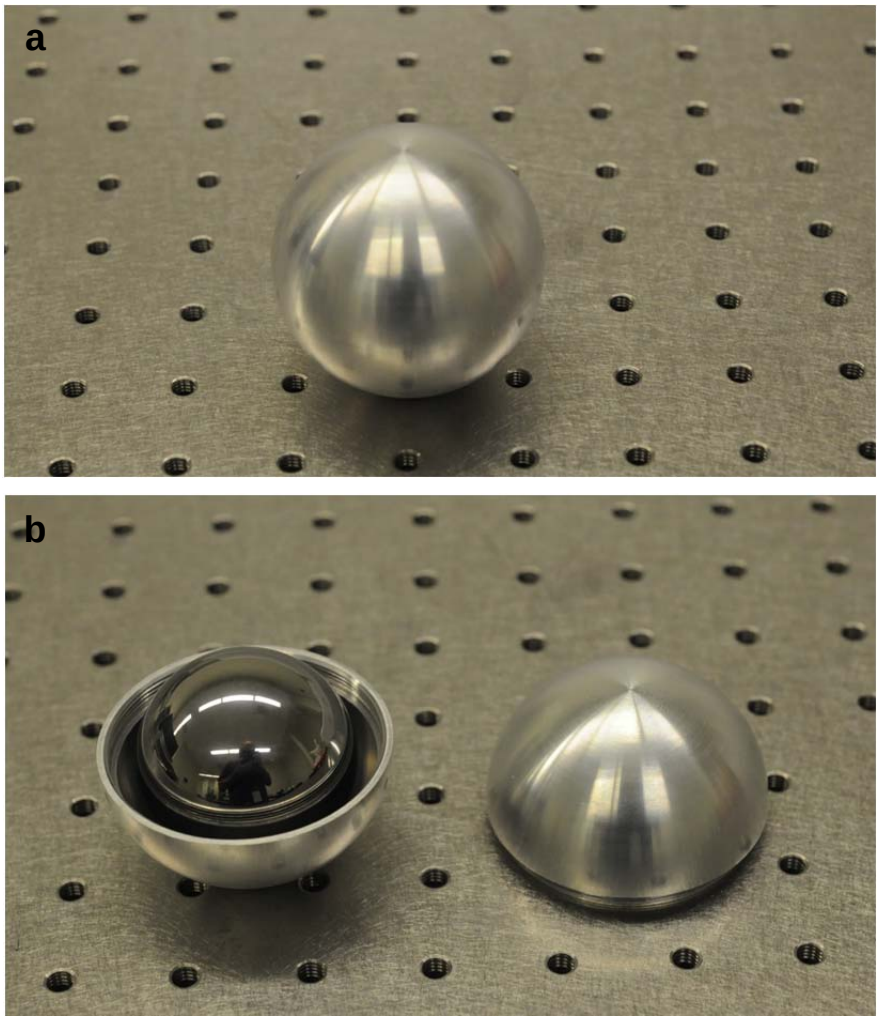

Supplemental Figure S4. (a) Photographs of a 60 mm diameter hollow alumina sphere. (b) Disassemble sphere with a ballast sphere inside. The sphere weight can be adjusted to exactly match that of the ice-shell-metal-core spheres, thus giving a more precise comparison of effect of the ice surface on the terminal velocity.

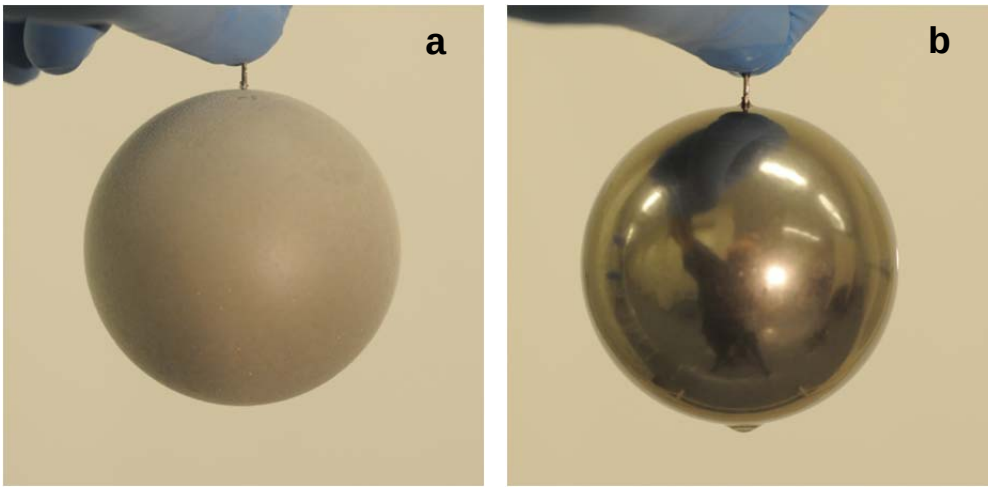

Supplemental Figure S5. Photographs of a 60 mm diameter steel sphere. (a) Sphere has been cooled to –20 ºC and then exposed to the laboratory atmosphere where a frost layer forms on the surface. (b) Sphere appearance after a brief wash with ethanol to remove the frost layer. The ethanol wets the sphere surface and prevents frost formation.

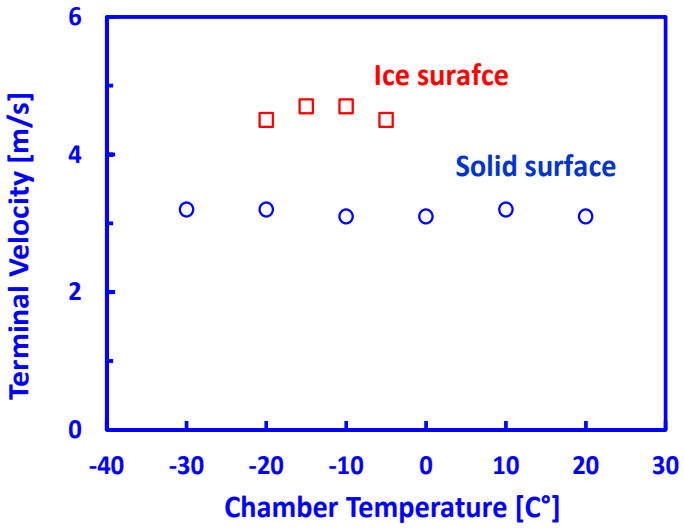

Supplemental Figure S6. Variation of the apparent terminal velocity of spheres in water with the temperature at which the spheres have been equilibrated. Results are given for a 60 mm diameter ice(metal) spheres (open squares, red) and a 60 mm diameter solid steel spheres (open circles, blue) of the same weight. For temperatures below zero the steel sphere surface is first defrosted by a brief wash with ethanol (see Fig. S5). Independent of the chamber temperature between –20 ºC to –5 ºC, the ice(metal) spheres are first conditioned at room temperature until the surface starts to melt so that the ice shell temperature is between –2 ºC to 0 ºC (Fig. S2).

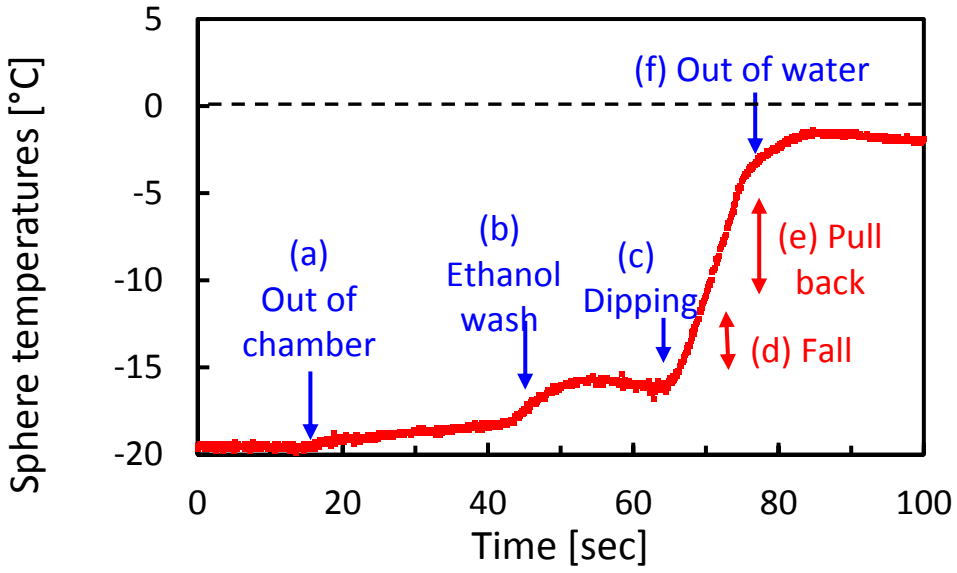

Supplemental Figure S7. Chronology of a cooled 60 mm diameter steel sphere monitored by the thermocouple probe mounted inside the steel sphere for the steps: (a) taking the sphere out of the chamber (chamber temperature –20 ºC); (b) brief wash with ethanol to defrost; (c) dipping in water; (d) fall to the bottom of the tank; (e) pull back of the sphere from the tank; (f) taken out of the water. The sphere temperature remains below zero.

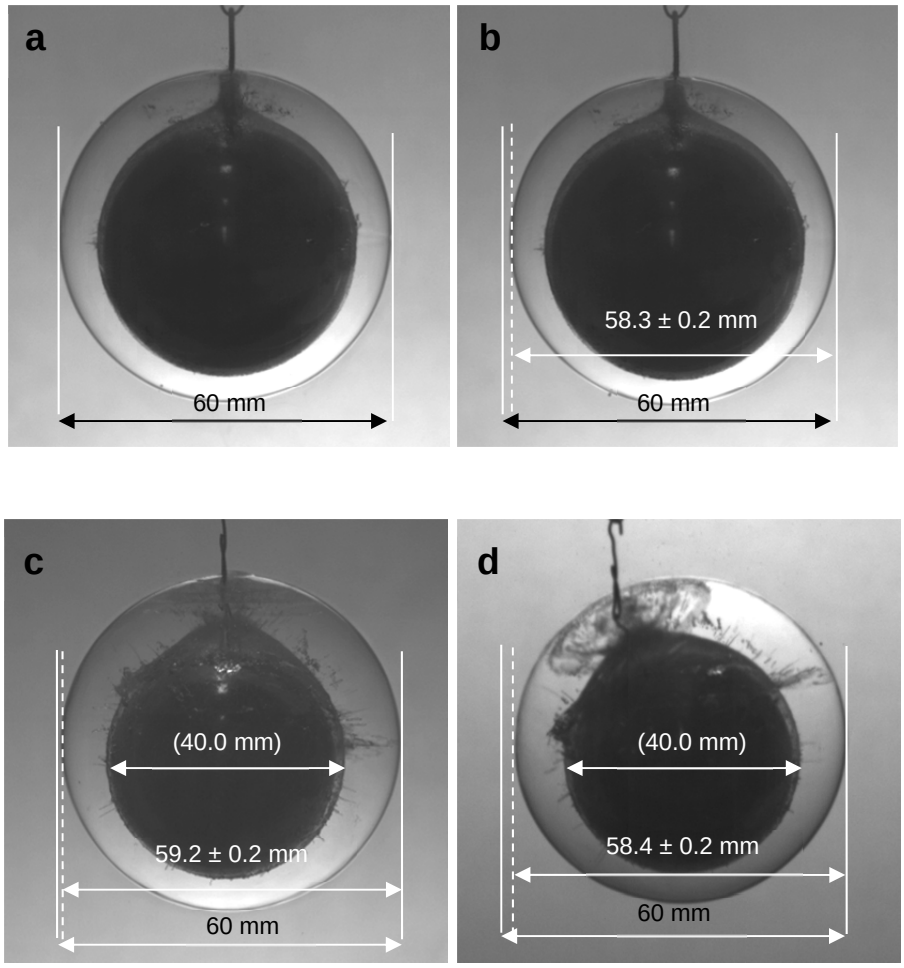

Supplemental Figure S8. High magnification high-speed camera snapshots used to estimate the ice(metal) sphere melting rate for a stationary (a, b) and a free falling sphere (c, d): (a) the stationary sphere shortly after immersion in water and (b) 20 seconds later. (c) The falling sphere at the moment of release at the top of the tank and (d) the same sphere 1.2 seconds later close to the bottom of the tank. An accurate estimate of the size change is to use the size of the metallic core sphere as scale.